Effects of Annealing Ambient on the Structural, Optical and Electrical Properties of TiO₂:Ge Thin Films

Lilian A Owino*, Sebastian Waita, Robinson J Musembi and Francis W Nyongesa
Department of Physics, University of Nairobi, P.O. Box 00100-30197, Nairobi, Kenya
*Corresponding author, e-mail: swanny@students.uonbi.ac.ke
Co-authors' e-mail addresses: swaita@uonbi.ac.ke; musembirj@uonbi.ac.ke;
fnyongesa@uonbi.ac.ke

Abstract

TiO_2, a semiconducting material with a wide energy band gap, has been researched intensively due to its interesting properties and many potential applications. The films properties can as well be modified by preparing the films under diverse ambient to suit diverse applications. In this work, the effects of the annealing atmosphere on the structural, optical and electrical properties of pure TiO_2 and TiO_2:Ge composite thin films deposited by sputtering from commercially available pure TiO_2 and TiO_2:Ge (85:15) targets respectively were studied. The films were deposited on fluorine doped tin oxide glass substrates by radio frequency magnetron sputtering technique at room temperature 23–25 °C and then annealed at 450 °C for one hour in three different atmospheres: air, argon and nitrogen. The XRD results revealed that, both pure TiO_2 and TiO_2:Ge thin films were crystalline and had a mixed phase of anatase and rutile regardless of the annealing ambient. The calculated crystallite sizes ranged between 19–21 nm with the particle sizes for TiO_2:Ge films being larger compared to pure TiO_2 as calculated from ImageJ software. Electrical measurements showed that the resistivity of as deposited pure TiO_2 films (about 13.03×10^{-2} Ω-cm) was greater than the TiO_2: Ge composite (5.91×10^{-2} Ω-cm). Furthermore, on annealing, pure TiO_2 had a resistivity of 9.47×10^{-2} Ω-cm–10.4×10^{-2} Ω-cm, while the TiO_2:Ge composite had a resistivity of 2.24×10^{-2} Ω-cm–3.61×10^{-2} Ω-cm depending on the annealing atmosphere. Variation of annealing atmosphere had minimal influence on the electrical resistivity of the films. The films annealed in nitrogen recorded the least resistivity values averaging about 5.86×10^{-2} Ω-cm, while those annealed in argon and air recorded a resistivity of 6.94×10^{-2} Ω-cm and 6.65×10^{-2} Ω-cm, respectively. The transmittance spectra showed that, all the annealed films were transparent in the visible region (400–700 nm) with a mean bandgap of 3.60 eV for each annealing atmosphere. It is recommended that films annealed in nitrogen atmosphere could be considered for potential applications in photovoltaics.

Keywords: Titanium dioxide; Germanium; Ambient; Structural; Optical, Electrical.

Introduction

Titanium dioxide is a wide bandgap semiconductor which has attracted great interest because of its unique characteristics such as its excellent transmittance in the visible region, high refractive index and dielectric constant, good thermal and chemical stability, non-toxicity and also its abundance on the earth surface (DeLoach et al. 1999). Thin films of TiO_2 have found many applications such as in solar cells, flat panel displays (Carp et al. 2004), sensors (Carmichael et al. 2013) and other optoelectronic devices. Although TiO_2 is

widely used in the above-mentioned applications, the efficiencies of the fabricated devices have generally been low. This is due to the wide bandgap of TiO_2 and its relatively low electron conductivity (Choi et al. 1994). Researchers have come up with a number of ways to counter these shortcomings among them being doping TiO_2 with metal and non-metal ions, dye sensitization (Diaz-Angulo et al. 2019), optimization of deposition parameters, fabrication of TiO_2 composites (Chatterjee 2008b), or producing defective TiO_2 by introducing Ti^{3+} and oxygen vacancies by reduction (Chatterjee 2008a, Stengl and Bakardjieva 2010, Zheng et al. 2013).

Doping and dye sensitization have proved to be among the effective approaches towards tailoring the properties of TiO_2. However, these approaches are faced with some drawbacks such as some dopants acting as recombination centres for the photogenerated charge carriers especially for transition metals like zinc, iron, and copper among others. Also, the instability of the organic complex in the dye together with charge transport still poses a significant challenge (Chatterjee et al. 2006). This therefore necessitates for other ways of optimizing the properties of TiO_2. Defective TiO_2 can also be produced by annealing in a hydrogen environment or in hydrogen plasma. Active metals such as aluminium and magnesium can also be used as reductants in obtaining defective TiO_2 (Naldoni et al. 2012). However, these methods are considered as harsh reductive conditions and instead, defective TiO_2 can easily be obtained by annealing amorphous TiO_2 nanoparticles in nitrogen, argon or in a vacuum (Tian et al. 2015). Recent research demonstrated that formation of TiO_2 composites nanostructures could also improve the properties of the semiconductor. Metals and non-metals nanoparticles are often introduced in TiO_2 matrix to increase the separation of photo-induced charge carriers during photocatalytic processes in areas of photocatalysis and solar energy conversion. Although many elements have been proposed for this purpose, carbon and its allotropes remain to be the primary choice because they exhibit a large electron storage capacity that may accept electrons excited by photons, thus retarding the recombination process (Woan et al. 2009). So far, composite film of graphene/TiO_2 has been used as a photoanode in the fabrication of DSSC and yielded a solar cell with improved efficiency (Tsai et al. 2011).

Germanium element, being among the carbon family, has also shown great potential when used as a composite with TiO_2 in fabrication of DSSC. Chatterjee (2008a) studied TiO_2:Ge nanocomposite as a photovoltaic material. It was noted that TiO_2:Ge composite is a promising material for fabrication of DSSC. Germanium exhibits a good electron transfer due to its narrow bandgap, and this widens its use in solar cells and in other optoelectronic devices. Also, germanium has a remarkable absorption in the infrared region, and also has a low sintering temperature which increases the inter-particle contact leading to improved electron transfer. Not much work has been done on TiO_2:Ge composite thin films, and therefore in the present study, the effects of annealing ambient (air, argon and nitrogen) on structural, optical, and electrical properties of TiO_2:Ge composite thin films prepared by radio-frequency magnetron sputtering method were studied. Alongside, pure TiO_2 thin films were also prepared for comparison.

Materials and Methods

Pure TiO_2 (99.99% purity) and TiO_2:Ge composite thin films were deposited on fluorine doped tin oxide glass substrates by radio frequency magnetron sputtering method using an Edwards Auto 306 deposition system. TiO_2 and TiO_2:Ge (85:15) composite disks, 125 inches thick were used as targets. The substrates were ultrasonically cleaned in ethanol, acetone and rinsed in distilled water, respectively. The cleaned substrates (1 cm by 1 cm by 20 mm) were then dried in ambient before deposition. Prior to the sputtering process, the auto 306 sputtering system was evacuated to a base pressure of 4.4×10^{-5} mbar using a turbo molecular pump to create a semi-vacuum. The target-substrate distance was maintained at about 20 cm for all the

depositions. Pre-sputtering was done for 10 minutes in pure argon to remove the surface contaminants from the target. The process pressure was maintained at 6.0×10^{-3} mbar. The deposition process was carried out for 1½ hours at room temperature (23.0–25.0 °C). The substrate was rotated at about 10 rounds per minute during deposition to enhance the film uniformity. The deposited thin films were thereafter annealed in three different atmospheres (air, argon and nitrogen) at 450 °C for one hour.

The crystallographic structures of the annealed films were analysed using the Bruker D2 PHASER diffractometer with CuK_α X-ray radiation (1.5418 Å) and readings were taken over the $10° < 2\theta < 80°$ range at a scan speed of 0.6 °/s and steps of 0.01°. Surface morphology of the deposited films was studied using Scanning Electron Microscopy (ZEISS ULTRA PLUS FEG SEM-Microscopes), while the optical and

electrical resistivity measurements of the films were done using UV-Vis-NIR 3700 double beam Shimadzu[TM] spectrophotometer and four-point probe (Jandel RM3-AR) method, respectively. The thickness of the annealed TiO_2:Ge thin film was estimated by simulating the transmittance data in scout software.

Results and Discussion
Structural and morphological characterization

Figure 1 shows the X-ray Diffraction (XRD) patterns for pure TiO_2 and TiO_2:Ge thin films deposited on FTO glass substrates at room temperature (23.0–25.0 °C), and later annealed in nitrogen, argon and air atmospheres. The XRD patterns were compared with the Joint Committee on Powder Diffraction Standards (JCPDS) database card No.21-1272 for anatase and 21–1276 for rutile (Waita et al. 2007).
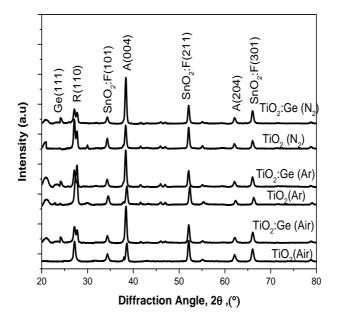

Figure 1: XRD patterns for TiO_2 and TiO_2:Ge thin films annealed in different atmospheres.

It was observed that, all the annealed films were crystalline and composed of anatase and rutile phases irrespective of the annealing atmosphere. A peak corresponding to the rutile phase appeared at 27 $^\circ$ (110) plane followed by a strong intensity peak at 38 $^\circ$ (004) plane which corresponds to the anatase phase. A minor peak corresponding to Ge was also observed at 24 $^\circ$ (111) in all TiO$_2$:Ge thin films. The presence of Ge and TiO$_2$ peaks showed that TiO$_2$:Ge thin films were composite in nature. Also, annealing the films in different atmospheres gave almost the same crystallinity with sharp peaks at (004) plane for pure TiO$_2$ as well as TiO$_2$:Ge thin films. The intensity of (110) plane for the rutile phase was higher in the pure TiO$_2$ films than TiO$_2$:Ge thin films annealed in different atmospheres. This suggests that the addition of Ge element in the TiO$_2$ lattice limits the formation of the rutile phase. TiO$_2$:Ge composite thin films peaks showed a higher intensity at 38 $^\circ$ (004) peak compared to those of TiO$_2$, and this was attributed to an improved crystallinity of the films. The XRD data was used to estimate the crystallite sizes for TiO$_2$:Ge thin films using the Debye-Scherrer's formula shown in Equation 1 (Arunachalam et al. 2015). The Full Width at Half Maximum (FWHM) values were obtained using the 38 $^\circ$ (004) peak since it was the most prominent.

$$D = \frac{K\lambda}{\beta COS\theta} \qquad [1]$$

Where $K = 0.9$ is the shape factor, λ is the wavelength used (0.15405), β is the full width at half maximum (FWHM) value and θ is the Braggs angle in radians. The crystallite size ranged between 19–21 nm.

Table 1: Crystallite sizes and full width at half maximum for TiO$_2$:Ge and TiO$_2$ thin films annealed in air, argon and nitrogen

Film	Annealed in air		Annealed in argon		Annealed in nitrogen	
	FWHM	Crystallite size (nm)	FWHM	Crystallite size (nm)	FWHM	Crystallite size (nm)
TiO$_2$	0.4401	19.11	0.4381	19.20	0.4329	19.43
TiO$_2$:Ge	0.4182	20.11	0.4105	20.87	0.3914	21.49

It was noted that the composite films had larger crystals compared to the pure TiO$_2$ films. Nitrogen annealed films recorded slightly bigger crystallite sizes to those films annealed in air. This was attributed to improved crystallinity of the films.

Figure 2 shows the SEM images for pure TiO$_2$ and TiO$_2$:Ge thin films annealed in nitrogen, argon and air, respectively. All the films showed a uniform structure without cracks or pinholes and well covered to the substrate. The homogeneous property makes the films suitable for use as a compact TiO$_2$ blocking layer in the fabrication of DSSC. TiO$_2$:Ge (85:15) films were composed of bigger particles compared to pure TiO$_2$ in all the samples. The films annealed in air were composed of small homogeneous particle sizes, while the films annealed in Ar and N$_2$ showed larger sizes. The increase in particle sizes for the films annealed in Ar and N$_2$ indicated an improved crystallinity of the films.
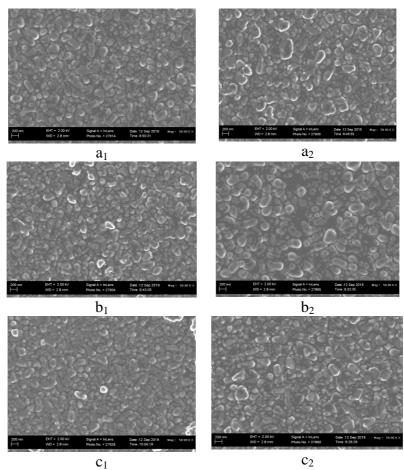
Figure 2: The SEM micrographs images for pure TiO_2 and TiO_2:Ge (85:15) annealed in different atmospheres. Images a_1, b_1 and c_1 are for pure TiO_2 annealed in nitrogen, argon and air, respectively, while a_2, b_2 and c_2 are films for TiO_2:Ge annealed in nitrogen, argon and air, respectively.

The particle sizes of the SEM images for the films were approximated using ImageJ software (Abràmoff et al. 2004). Table 2 summarizes the particle sizes of the films as approximated by ImageJ software.

Table 2: The particle sizes of pure TiO_2 and TiO_2: Ge (85:15) annealed in N_2, Ar and air

Film	Annealed in N_2 Grain size (nm) (±0.01)	Annealed in Ar Grain size (nm) (±0.01)	Annealed in Air Grain size (nm) (±0.01)
Pure TiO_2	33.69	32.10	30.83
TiO_2: Ge (85:15)	38.26	36.85	31.85

It was observed that TiO_2: Ge (85:15) films (a_2, b_2, c_2) were composed of bigger particles compared to pure TiO_2 (a_1, b_1, c_1) in all samples. It was confirmed that the films annealed in N_2 showed bigger particle sizes than those annealed in air and Ar. The trend of the results agreed well with the calculated crystallite sizes from XRD results as shown in Table 1.

Optical characterization
Visual observations

In terms of physical appearance, TiO_2 and TiO_2:Ge thin films without thermal treatment were opaque, but after thermal treatment at 450 °C for 1 hour in air, they became transparent. However, the colour of the films annealed in nitrogen and argon gases turned to dark brown after annealing. This colour change could be attributed to the oxygen loss from titania to form oxygen vacancy defects (Ghicov et al. 2006).

Film thickness

Table 3 shows the variations of thickness for TiO_2:Ge films with the annealing atmosphere as obtained from SCOUT software.

The change in the film thickness was almost insignificant, and this may be because the films were subjected to equal deposition time. However, from Table 3, TiO_2:Ge composite films appeared to be more thicker than pure TiO_2 films. This may be attributed to the inclusion of Ge element in TiO_2 matrix which improved the films compactness.

Table 3: Variation of thickness for TiO_2 and TiO_2: Ge composite thin films annealed in air, nitrogen and argon

Film	Annealed in Air Thickness (nm)) ± 0.1	Annealed in N₂ Thickness(nm) (±0.1)	Annealed in Ar Thickness (nm) ± 0.1
Pure TiO_2	176.6	179.4	177.3
TiO_2: Ge (85:15)	178.6	181.7	180.5

Transmittance

The influence of annealing atmosphere as well as that of incorporating Ge element in the TiO_2 lattice on the transmittance of the films was analysed and discussed as follows. Figure 3 shows the transmittance spectra for pure TiO_2 and TiO_2:Ge films annealed in air, Ar and N_2.

It was be observed from Figure 3 that all the films were transparent in the visible region. The transmission in the visible region decreased substantially at shorter wavelength (< 400 nm) near the ultraviolet range for all the films with maximum absorbance occurring in the wavelength 300–400 nm. This could be due to multiple reflections by the glass and films, and also due to absorption of light by the films and the glass (El-Raheem and Al-Baradi 2013). Pure TiO_2 films showed the highest transmittance in all the films averaging about 88%, 80%, and 70% for the films annealed in air, argon, and nitrogen, respectively in the wavelength's region of 400– 700 nm. The addition of Ge in TiO_2 lattice to form a composite resulted to a decrease in the transmittance by about 5–10%. This could be possibly due to the increased surface roughness in the films which promoted the surface scattering of light (Yousif et al. 2016). The SEM images for TiO_2:Ge in Figure 2 showed that the films were made up of a mixture of big and small particle sizes. This could be an indication of improved surface roughness of the films. Air annealed films showed the highest transmittance averaging about 79%, while the films annealed in nitrogen recorded the lowest transmittance averaging about 73%. The lowest transmittance was associated with films colour change which turned dark brown upon annealing the films in N_2 gas. The dark brown colour suggests a higher absorption in the visible region (Folger et al. 2017), and also could be attributed to the oxygen loss from titania to form oxygen vacancy defects (Ghicov et al. 2006). A similar colour change effect had also been reported by Gamboa and Pasquevich (1992) in their study on the effect of chlorine atmosphere on TiO_2 anatase-rutile phase .
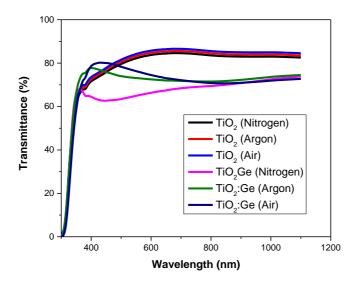
Figure 3:   Transmittance spectra for pure TiO_2 and TiO_2:Ge thin films annealed in different atmospheres.

Energy bandgap

The energy bandgap for pure TiO_2 and TiO_2:Ge composite was determined using the plot of $(\alpha h v)^{1/2}$ against hv. The bandgap was estimated by extrapolating the linear part with the hv axis and calculated using Equation [2], the Tauc's equation (Dolgonos et al. 2016).

$$Ahv = A (hv\text{-}E_g)^{\,n} \qquad [2]$$

In the above equation, α is the absorption coefficient, E_g is the bandgap, A is a constant which depends on the material used, $h\,\upsilon$ is the photon energy and n is the transition type. n is 2, ½, 3 and 2/3 for indirect allowed, direct allowed, indirect forbidden and direct forbidden transitions, respectively (Tang et al. 1994). Figure 4 shows that pure TiO_2 recorded bandgap averaging about 3.62, 3.65, and 3.66 eV for the films annealed in N_2, Ar, and air atmospheres, respectively. The bandgap decreased upon introduction of Ge element in TiO_2 matrix.

The reduction in energy bandgap could be due to the introduction of Ge impurity in either valence or conduction bands for pure TiO_2 which created a tail energy levels that reduces bandgaps (Ayieko et al. 2012). Also, this could be explained by the large crystallite sizes recorded by TiO_2:Ge films as confirmed from the XRD results discussed above. The energy bandgap in thin films have an inverse relation to crystallite size, and therefore this implies that the decreasing bandgap is due to an increase in Ge-TiO_2 crystallite sizes (Goh et al. 2010). A similar observation was made by Liu et al. (2008) in his study on the effect of doping nitrogen in the TiO_2 by radio frequency sputtering. Nitrogen and Ar annealed films showed lower bandgap values, an observation which was attributed to the development of oxygen vacancies. The oxygen vacancies created by annealing TiO_2:Ge in argon and nitrogen could have resulted in Ti^{3+} states which may be used as intrinsic donors to narrow the bandgap of titania such that they can act as n-type donors. Air atmosphere is composed mainly of O_2 and therefore, the oxygen vacancies remained almost constant when the films were annealed in air hence a higher bandgap (Albetran et al. 2016).
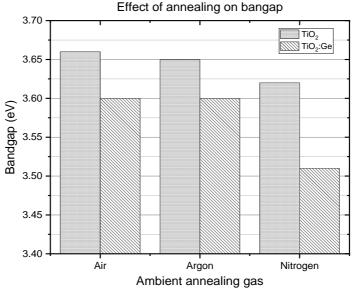
Figure 4: A histogram showing the bandgap variation for TiO$_2$ and TiO$_2$:Ge composite thin films annealed in air, argon and nitrogen gases.

Refractive index

Figure 5 shows the refractive index for TiO$_2$:Ge thin films annealed in air, N$_2$, and Ar atmospheres. It was noted that there was a generally high refractive index in the range 400–700 nm which is the visible region in all the films. However, the refractive index decreased as the wavelength increased towards the infrared region of the solar spectrum, and this could be due to lower energy associated with longer wavelengths. The films annealed in N$_2$ gas showed the highest refractive index, followed by those annealed in Ar and air, respectively. This variation could be attributed to the difference in the film density. TiO$_2$:Ge films annealed in N$_2$ were denser than those annealed in Ar and air. A thick layer is likely to be more compact and denser hence an increase in refractive index. The dense material has a high refractive index since more electric dipoles are activated when the material is exposed to the electric field of the incoming light (Aksay and Altıokka 2007).

The dependence of refractive index on the film porosity could be explained using the Lorentz-Lorenz relation which is defined as the ratio of average film density to bulk density (Pulker 1979, Waita et al. 2007).

$$P = \frac{\rho_f}{\rho_m} = (1 - \frac{n^2_f - 1}{n^2_f + 2} \cdot \frac{n^2_m + 2}{n^2_m - 1} \qquad [3]$$

Where n_m and n_f are the refractive indices of dense TiO$_2$ anatase phase (2.46) and that of the deposited films (TiO$_2$:Ge), respectively. Using the relation above, the calculated porosity for the TiO$_2$:Ge films annealed in air, argon and nitrogen were 18.3%, 11.4% and 10.8%, respectively.
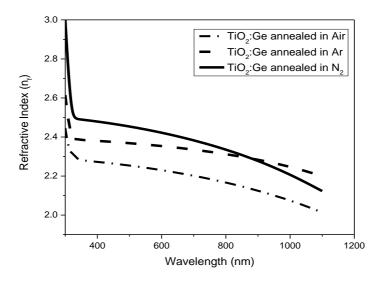
Figure 5: Dependence of refractive index on annealing atmosphere for TiO_2:Ge thin films.

Electrical characterization
Resistivity for pure TiO_2 and TiO_2:Ge composite thin films

The resistivity for pure TiO_2 and TiO_2:Ge thin films annealed in different atmospheres: air, Ar and N_2 was measured using a four-point probe method. Figure 6 shows a histogram summarizing the resistivity of the films for as-deposited and those annealed in different ambient.
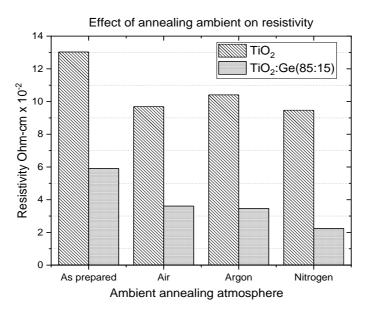

Figure 6: A histogram illustrating the resistivity for as-deposited and annealed TiO_2 and TiO_2:Ge thin films.

The annealed films recorded a resistivity of the same order (10^{-2}) irrespective of the annealing atmosphere with an exception of the films annealed in argon gas which recorded a resistivity of order 10^{-1}. This possibly suggests that annealing atmosphere had minimal influence on the resistivity of the films. However, from the histogram, the films annealed in nitrogen showed the least resistivity value compared to those annealed in air and argon. This could be attributed to the formation of additional oxygen vacancies during the annealing process in N$_2$ since it is an oxygen deficiency environment. These O$_2$ vacancies acted as donor centres for electrons hence resulting in a lower resistivity (Tong et al. 2011). It was also noted that TiO$_2$:Ge composite films had a lower resistivity compared to pure TiO$_2$ film. This could be attributed to improved crystallinity as a result of the increase in crystallite sizes of TiO$_2$:Ge. The XRD results confirmed that indeed, there was an increase in crystallite sizes of the films from 19 to 21 nm after incorporating Ge in TiO$_2$ matrix. Increase in grain size results to a decrease in the grain boundaries, which increases the flow of electrons hence a reduction in resistivity (Biju and Jain 2008).

Conclusion

Pure titanium dioxide (TiO$_2$) and titanium-germanium (TiO$_2$:Ge) composite thin films were successfully deposited using rf magnetron sputtering method. TiO$_2$ and TiO$_2$:Ge composite thin films were found to be generally transparent in the visible region. It was found that introduction of Ge element in TiO$_2$ matrix had a positive influence on both the optical and electrical properties of the films. TiO$_2$: Ge (85:15) recorded a lower transmittance average of 70% in wavelengths 400–700 nm compared to the pure TiO$_2$. The bandgap decreased from 3.64 eV to 3.56 eV, while the electrical resistivity decreased from 11.01×10^{-2} Ω-cm to 5.85×10^{-2} Ω-cm upon introduction of Ge in TiO$_2$ structure. Structurally, from the XRD analysis, introduction of Ge in TiO$_2$ improved the crystallinity of the films. Different annealing atmospheres had minimal effects on the electrical and structural properties of TiO$_2$:Ge

thin films. However, annealing the films in different ambient showed a great effect on their optical properties. Nitrogen annealed films recorded a lower bandgap averaging about 3.55 eV with a good transmittance in the visible region. This was attributed to formation of oxygen vacancies in TiO$_2$ structure. Generally, the films annealed in oxygen deficient environment (N$_2$) gave the best optical and electrical properties with the largest particle sizes. It was therefore recommended that TiO$_2$:Ge thin films annealed in nitrogen atmosphere could be considered for applications such as photoanode in dye-sensitized solar cells, transparent conduction oxides or even compact blocking layer in dye-sensitized solar cells among others.

References
Abràmoff MD, Magalhães PJ and Ram SJ 2004 Image processing with ImageJ. *Biophotonics Int.* 11: 36–42.

Aksay S and Altıokka B 2007 Effect of substrate temperature on some of the optical parameters of CuInS$_2$ films. *Phys. Status Solidi C* 4: 585–588.

Albetran H, O'Connor BH and Low IM 2016 Effect of calcination on band gaps for electrospun titania nanofibers heated in air–argon mixtures. *Mater. Des.* 92: 480–485.

Arunachalam A, Dhanapandian S, Manoharan C and Sivakumar G 2015 Physical properties of Zn doped TiO$_2$ thin films with spray pyrolysis technique and its effects in antibacterial activity. *Spectrochim. Acta. A. Mol. Biomol. Spectrosc.* 138: 105–112.

Ayieko CO, Musembi RJ, Waita SM, Aduda BO and Jain PK 2012 Structural and optical characterization of nitrogen-doped TiO$_2$ thin films deposited by spray pyrolysis on fluorine doped tin oxide

(FTO) coated glass slides. *Int. J. Energy Eng.* 2: 67–72.

Biju KP and Jain MK 2008 Effect of crystallization on humidity sensing properties of sol–gel derived nanocrystalline TiO_2 thin films. *Thin Solid Films* 516: 2175–2180.

Carmichael P, Hazafy D, Bhachu DS, Mills A, Darr JA and Parkin IP 2013 Atmospheric pressure chemical vapour deposition of boron doped titanium dioxide for photocatalytic water reduction and oxidation. *Phys. Chem. Chem. Phys.* 15: 16788–16794.

Carp O, Huisman CL and Reller A 2004 Photoinduced reactivity of titanium dioxide. *Prog. Solid State Chem.* 32: 33–177.

Chatterjee S 2008a Titania–germanium nanocomposite as a photovoltaic material. *Sol. Energy* 82: 95–99.

Chatterjee S 2008b Titania–germanium nanocomposite as a photovoltaic material. *Sol. Energy* 82: 95–99.

Chatterjee S, Goyal A and Shah SI 2006 Inorganic nanocomposites for the next generation photovoltaics. *Mater. Lett.* 60: 3541–3543.

Choi W, Termin A and Hoffmann MR 1994 The role of metal ion dopants in quantum-sized TiO_2: correlation between photoreactivity and charge carrier recombination dynamics. *J. Phys. Chem.* 98: 13669–13679.

DeLoach JD, Scarel G and Aita CR 1999 Correlation between titania film structure and near ultraviolet optical absorption. *J. Appl. Phys.* 85: 2377–2384.

Diaz-Angulo J, Arce-Sarria A, Mueses M, Hernandez-Ramirez A and Machuca-Martinez F 2019 Analysis of two dye-sensitized methods for improving the sunlight absorption of TiO_2 using CPC photoreactor at pilot scale. *Mater. Sci. Semicond. Process.* 103: 104640.

Dolgonos A, Mason TO and Poeppelmeier KR 2016 Direct optical band gap measurement in polycrystalline semiconductors: A critical look at the Tauc method. *J. Solid State Chem.* 240: 43–48.

El-Raheem MA and Al-Baradi AM 2013 Optical properties of as-deposited TiO_2 thin films prepared by DC sputtering technique. *Int. J. Phys. Sci.* 8: 1570–1580.

Folger A, Kalb J, Schmidt-Mende L and Scheu C 2017 Tuning the electronic conductivity in hydrothermally grown rutile TiO_2 Nanowires: Effect of heat treatment in different environments. *Nanomaterials* 7: 289.

Gamboa JA and Pasquevich DM 1992 Effect of chlorine atmosphere on the anatase-rutile transformation. *J. Am. Ceram. Soc.* 75: 2934–2938.

Ghicov A, Tsuchiya H, Macak JM and Schmuki P 2006 Annealing effects on the photoresponse of TiO_2 nanotubes. *Phys. Status Solidi A* 203: R28–R30.

Goh ES, Chen TP, Sun CQ and Liu YC 2010 Thickness effect on the band gap and optical properties of germanium thin films. *J. Appl. Phys.* 107: 024305.

Liu B, Wen L and Zhao X 2008 The structure and photocatalytic studies of N-doped TiO_2 films prepared by radio frequency reactive magnetron sputtering. *Sol. Energy Mater. Sol. Cells* 92: 1–10.

Naldoni A, Allieta M, Santangelo S, Marelli M, Fabbri F, Cappelli S, Bianchi CL, Psaro R and Dal Santo V 2012 Effect of nature and location of defects on bandgap narrowing in black TiO_2 nanoparticles. *J. Am. Chem. Soc.* 134: 7600–7603.

Pulker HK 1979 Characterization of optical thin films. *Appl. Opt.* 18: 1969.

Stengl V and Bakardjieva S 2010 Molybdenum-doped anatase and its extraordinary photocatalytic activity in the degradation of orange II in the UV and vis regions. *J. Phys. Chem. C* 114: 19308–19317.

Tang H, Berger H, Schmid PE and Levy F 1994 Optical properties of anatase (TiO_2). *Solid State Commun.* 92: 267–271.

Tian M, Mahjouri-Samani M, Eres G, Sachan R, Yoon M, Chisholm MF, Wang K, Puretzky A, Rouleau CM and Geohegan DB 2015 Structure and formation mechanism of black TiO_2 nanoparticles. *ACS Nano* 9: 10482–10488.

Tong H, Deng Z, Liu Z, Huang C, Huang J, Lan H, Wang C and Cao Y 2011 Effects of post-annealing on structural, optical and electrical properties of Al-doped ZnO thin films. *Appl. Surf. Sci.* 257: 4906–4911.

Tsai TH, Chiou SC and Chen SM 2011 Enhancement of dye-sensitized solar cells by using graphene-TiO$_2$ composites as photoelectrochemical working electrode. *Int. J. Electrochem. Sci.* 6: 3333–3343.

Waita SM, Aduda BO, Mwabora JM, Granqvist CG, Lindquist SE, Niklasson GA, Hagfeldt A and Boschloo G 2007 Electron transport and recombination in dye sensitized solar cells fabricated from obliquely sputter deposited and thermally annealed TiO$_2$ films. *J. Electroanal. Chem.* 605: 151–156.

Woan K, Pyrgiotakis G and Sigmund W 2009 Photocatalytic carbon-nanotube–TiO$_2$ composites. *Adv. Mater.* 21: 2233–2239.

Yousif A, Aadim DK and Al-Isawi N 2016 Influence of Ag doping on optical properties of nanocrystalline titanium dioxide prepared by PLD. *IOSR J. Appl. Phys.* 08: 50–56.

Zheng Z, Huang B, Meng X, Wang J, Wang S, Lou Z, Wang Z, Qin X, Zhang X and Dai Y 2013 Metallic zinc-assisted synthesis of Ti^{3+} self-doped TiO$_2$ with tunable phase composition and visible-light photocatalytic activity. *Chem. Commun.* 49: 868–870.